Capacitive Touch Panel with Low Sensitivity to Water Drop employing Mutual-coupling Electrical Field Shaping Technique

Longjie Zhong, *Student Member, IEEE,* Xinquan Lai, *Member, IEEE,* Donglai Xu, *Senior Member, IEEE,* Xinqin Liao, Chuanshi Yang, Zhongyuan Fang, *Student Member, IEEE,* and Yuanjin Zheng, *Senior Member, IEEE*

***Abstract*—This paper proposes a novel method to reduce the water interference on the touch panel based on mutual-capacitance sensing in human finger detection. As the height of a finger (height>10mm) is far larger than that of a water-drop (height<1mm), if the density distribution of electrical field of the touch panel's sensing cell is high in the high-height space (height>10mm) and low in the low-height space (height<1mm), the sensing cell can be designed to distinguish the finger from the water-drop. To achieve this density distribution of the electrical field, the Mutual-coupling Electrical Field Shaping (MEFS) technique is employed to build the sensing cell. The drawback of the MEFS sensing cell is large parasitic capacitance, which can be overcome by a readout IC with low sensitivity to parasitic capacitance. Experiments show that the output of the IC with the MEFS sensing cell is 1.11V when the sensing cell is touched by the water-drop and 1.23V when the sensing cell is touched by the finger, respectively. In contrast, the output of the IC with the traditional sensing cell is 1.32V and 1.33V when the sensing cell is touched by the water-drop and the finger, respectively. This demonstrates that the MEFS sensing cell can better distinguish the finger from the water-drop than the traditional sensing cell does.**

***Index Terms*—Water interference, mutual capacitance, touch sensing, touch panel, capacitive readout circuit, fully differential, switched-capacitor circuits, OSA technique.**

I. Introduction

Touch sensing is widely used as a touch user interface for smart phones, tablets and household applications. Mutual-capacitance sensing technique is more popular than self-capacitance sensing technique in touch panel/screen applications due to its ability for multi-touch detection [1], [2]. However, the mutual-capacitance sensing technique has the limitation that reading the sensing cells in the presence of water-drop is difficult [3]-[6]. This is because the mutual-capacitance sensing technique is based on the detection of the dielectric constant of the space between two adjacent sensing plates of a sensing cell. The dielectric constant of the water is similar to that of the finger. So it is very hard for the mutual-capacitance sensing cell to distinguish the finger from the water-drop.

In general, to reduce the water-drop interference, the touch panel is designed by combining the mutual-capacitance sensing technique with the self-capacitance sensing technique. Normally, in one detecting operation, the sensing cells are firstly activated by self-capacitance sensing and then activated by the mutual-capacitance sensing. By analyzing the data from the two different detection processes, the water-drop is distinguished [3]. This is because the self-capacitance sensing technique detects the capacitance of the human body, whose value is far larger than the value of the capacitance of a water-drop. However, this method is still unable to reduce the water-drop interference in some specific cases and the hardware cost is high [4]. Another popular method to reduce the water-drop interference is to design the sensing cell in the form of a sealed box with elastic cavity inside. When the finger touches the surface of the box, the cavity is compressed and thus the capacitance of the sensing cell is changed. In this design, the mutual-coupling electrical field is completely restricted inside the box, so it is free from any effect from the water-drop outside the box [5], [6]. However, the elastic cavity inside the sensing cell requires very complex manufacturing process and the sensing cell based on this method is not easy to achieve the thickness required.

In this paper, a novel method to reduce the water-drop interference is proposed. This method distinguishes the human finger from the water drop by their physical dimensions. The finger is a cylinder with its height being more than 10mm, while that of the water-drop is only about 1mm. If the density distribution of electrical field of sensing cell is high in the high-height space (height >10mm) and low in the low-height space (height <1mm), the sensing cell would be less sensitive to the water-drop than it does to the finger, and thus the water-drop interference is reduced. To achieve the above electrical field distribution, the mutual-coupling electrical field shaping (MEFS) technique is adopted to build the sensing cell.

The rest of the paper is organized as follows. In the section II, the principle of the MEFS sensing cell is described. In the section III, the process for the finger

This work was supported in part by the National Natural Science Foundation of China (NSFC) under Grant 61771363, and in part by the China Scholarship Council (CSC) under Grant 201706960042, and in part by National Research Foundation of Singapore under Grant No. NRF-CRP11-2012-01.

L. Zhong and X. Lai are with the Institute of Electronic Computer-Aided Design, Xidian University, Xi'an 710071, China, and also with the Key Laboratory of High-Speed Circuit Design and Electromagnetic Compatibility, Ministry of Education, Xi'an 710071, China (e-mail: zhonglongjie4213@126.com; xqlai@mail.xidian.edu.cn).

D. Xu is with the School of Science and Engineering, Teesside University, Middlesbrough TS1 3BA, U.K., and also with the School of Electrical and Electronic Engineering, Wuhan Polytechnic University, Wuhan 430048, China(e-mail: d.xu@tees.ac.uk).

X. Liao, C. Yang, Z. Fang, and Y. Zheng are with VIRTUS, School of Electrical and Electronics Engineering, Nanyang Technological University, Singapore (liaoxinqin677@163.com; yjzheng@ntu.edu.sg; E150204@e.ntu.edu.sg; zfang005@e.ntu.edu.sg).

detection with reduced water-drop interference is illustrated and the circuit solution to the drawback of the MEFS sensing cell is described. In the section IV, the physical verification and measurement results are presented. Finally, the conclusions are drawn in the section V.

II. SENSING CELL PHYSICS

The differences between the water-drop and the human finger, which may be utilized by the sensing cell to distinguish them, are analyzed in detail as follows.

Firstly, they are different in physical dimension. This is a very reliable criteria to distinguish the finger from the water-drop. In daily use, the water-drop splashing to the surface of the touch panel mainly comes from the wet finger or steam. Thus, the amount of the water-drop is rather small and the height of the water-drop is much smaller than that of the finger. In general, the height of a water-drop is less than 1mm and the height of the finger is more than 10mm.

Secondly, the finger and the water-drop are different in coupling-capacitance to the electrical ground of power system. The finger couples with the environment via the whole human body whose superficial area is far larger than that of the water-drop. Therefore the finger is easier to couple with electrical ground of power system of the touch panel than the water-drop is, which means that the self-capacitance of the finger is much larger than that of the water-drop. This characteristic is very significant for self-capacitance sensing cell to distinguish the finger from the water-drop. However, this characteristic does not make any difference in mutual-capacitance sensing.

Thirdly, the finger and the water-drop are different in dynamics. The finger is always moving when the sensing cell is operated, while the water-drop is mostly static. So a band-pass filter can be used to distinguish the moving finger from the static water-drop. This criteria is reliable except for the situation where the water-drop is moved by the finger.

In overall consideration of detection robustness, the first criteria (physical dimension) is chosen and it is the basis on which the MEFS sensing cell is designed.

The traditional mutual-capacitance sensing cell shown in Fig.1. (a) is composed of two sensing plates: Plate_A on one side and Plate_B on the other side [7], [8]. According to the Maxwell's law and numerical analysis, the mutual-capacitance C_{T0} of this sensing cell is determined by the dielectric constant and the intensity of the mutual-coupling electrical field in the space between the two sensing plates. As the mutual-coupling electrical field is the strongest in the low-height space, the water-drop on the surface of the sensing cell will dominate the mutual-capacitance C_{T0}. In other words, if the sensing cell is covered by a water drop, the value of C_{T0} will not change regardless of the sensing cell being touched by the finger or not.

The traditional differential mutual-capacitance sensing cell shown in Fig.1. (b) is composed of three plates: Plate_A, Plate_B and Plate_Ref [9]. The mutual-capacitance between Plate_A and Plate_Ref is C_{T1}, and the mutual-capacitance between Plate_B and Plate_Ref is C_{T2}. When the water-drop covers the sensing cell, the capacitance brought by the water-drop is converted to the common-mode part of C_{T1} and C_{T2}, and the capacitance brought by the finger is converted to the differential part of C_{T1} and C_{T2}. So the finger is detectable in the presence of the water-drop. However, if the water-drop is not evenly distributed, e.g., the water-drop is on one side (Plate_A) and the finger is on the other side (Plate_B), it is still hard for this sensing cell to distinguish the finger from the water-drop.

The proposed MEFS sensing cell shown in Fig.1. (c) is composed of five plates: Plate_A, Plate_B, Plate_Ref and two ground plates. The mutual-capacitance between Plate_A and Plate_Ref is C_1, and the mutual-capacitance between Plate_B and Plate_Ref is C_2. The mutual-coupling electrical field between Plate_A and Plate_Ref is shaped by a ground plate, so does the electrical field between the Plate_B and Plate_Ref. Thus the strong mutual-coupling electrical field in the low-height space is guided to the ground by ground plate, while the mutual-coupling electrical field in the high-height space is kept. This means that the mutual capacitances C_1 and C_2 are dominated by the capacitance introduced by the electrical field in the high-height space, as the capacitance introduced by electrical field in the low-height space is converted to the capacitances C_{P1} and C_{P2} which are grounded and do not affect the mutual capacitances.

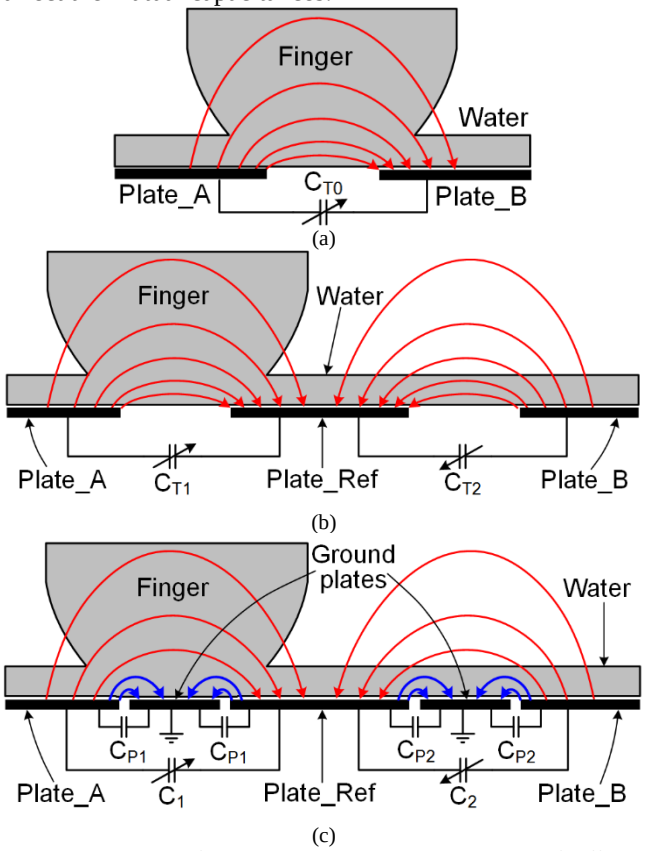

Fig. 1. The electrical field distribution and equivalent circuit of different sensing cells with the presence of water and finger. (a) Traditional mutual-capacitance sensing cell. (b) Traditional differential mutual-capacitance sensing cell. (c) The MEFS sensing cell.

The numerical analyses of the traditional differential mutual-capacitance sensing cell and the MEFS sensing cell are shown in Fig.2. (a) and Fig.2. (b), respectively (only one side is shown, i.e., Plate_A and Plate_ref). The vector maps clearly show that, by adding ground plate, the high

density mutual-coupling electrical field in the low-height space (dashed box of Fig.2. (b)) is guided to the ground. So in the water contacting area (space with height smaller than 1mm), the mutual-coupling electrical field between the two sensing plates (Plate_A and Plate_Ref) no longer exists. Meanwhile, in the finger contacting area (space with height larger than 10mm), the mutual-coupling electrical field is not significantly reduced.

The physical layouts of the touch panels based on the traditional differential sensing cell and the MEFS sensing cell are shown in Fig. 3(a) and Fig. 3(b), respectively. The yellow diamonds labeled "1" are Plate_ref. The blue diamonds labeled "2" and the pink diamonds labeled "3" are Plate_A and Plate_B, respectively. The grey diamonds labeled "4" are the ground plate. The cover area of a single sensing cell is marked by the square with black dash line and the cover area of the finger is marked by a circle with black dash line, as shown in Fig. 3. The size of the sensing cell is set to a value no larger than the cross section of a finger, in order to make sure there is at least one complete sensing cell fully covered by a finger of any size, so that the change of the finger size wouldn't have influence on the sensitivity of the sensing cell.

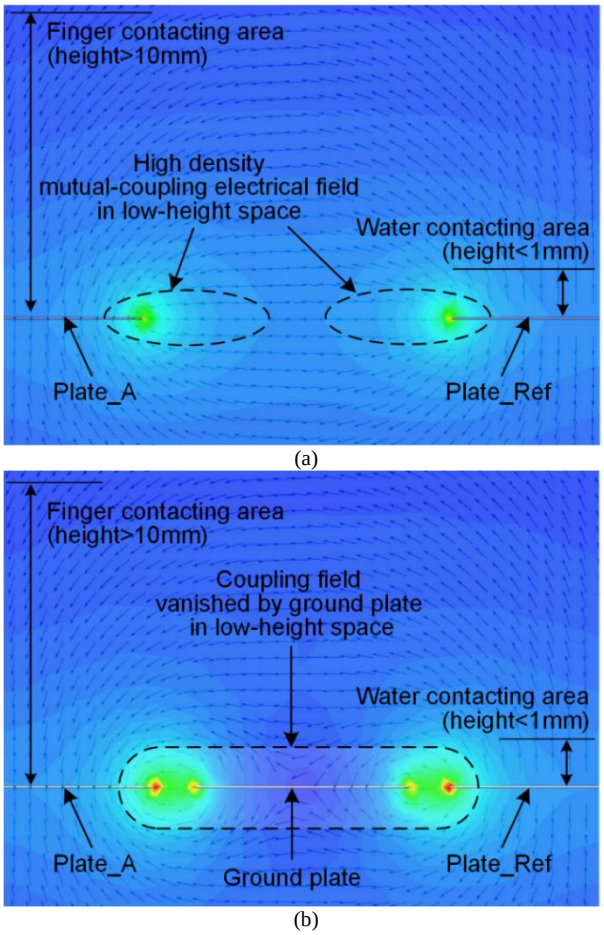

Fig. 2 The vector and color maps of the electrical field distribution of different sensing cells. (a) Traditional mutual-capacitance sensing cell. (b) The MEFS sensing cell.

In a single sensing cell, the mutual capacitance between the sensing plates "1" and "2" is C1, and the mutual capacitance between the sensing plates "1" and "3" is C2. The numerical analysis shows that, when the surface of the sensing cell is untouched, covered with water-drop and touched by the finger, the values of the capacitances of the traditional differential sensing cell are 309.1fF, 636.3fF and 641.5fF, respectively, as shown in Fig. 4 (a). For the MEFS sensing cell, these values are 24.4fF, 144.8fF and 213.1fF, respectively, as shown in Fig. 4 (b). Similar to the concept "dynamic range" of an amplifier [16], the percentage difference is used to quantify how well the water-drop and the finger is distinguished, which is defined as the difference value of two mutual capacitances divided by the maximum value of the capacitances. For traditional structure, the percentage difference is,

$$\Delta C_{Normal} = \frac{641.5 - 636.3}{641.5} = 0.8\% \quad (1)$$

For MEFS based structure, the percentage difference is

$$\Delta C_{MCEFS} = \frac{213.1 - 144.8}{213.1} = 32.4\% \quad (2)$$

It is obvious that it is very hard to use the traditional sensing cell to distinguish the finger from the water-drop as the percentage difference is only 0.8%, which requires high dynamic range circuit to process. However, for the MEFS sensing cell, the percentage difference increases by 32dB (from 0.8% to 32.4%), which significantly relaxes the dynamic range requirement of circuit.

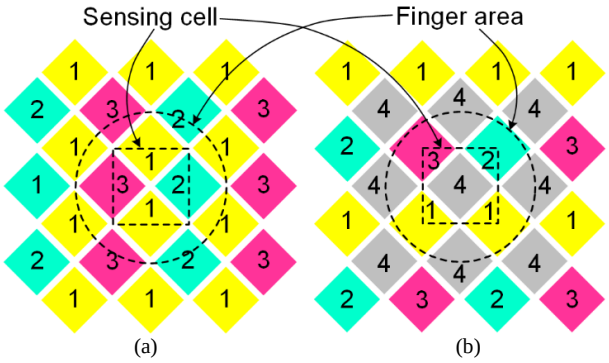

Fig. 3. Layouts of the touch panels based on (a) the differential mutual-capacitance sensing cell and (b) the MEFS sensing cell

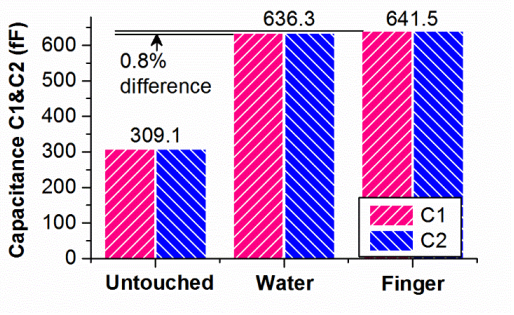

(a)

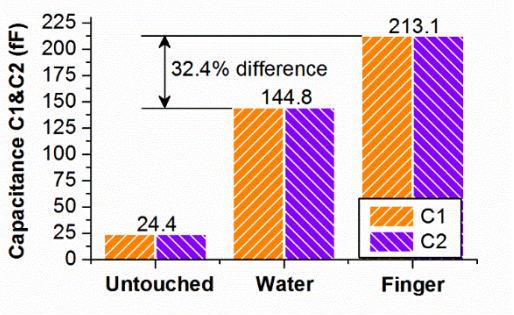

(b)

Fig. 4. The numerical results of the mutual capacitances of the sensing cells in different statuses: untouched, covered by the water-drop and touched by the finger. (a) The traditional differential sensing cell. (b) The MEFS sensing cell.

III. DETECTING PROCESS AND CIRCUIT IMPLEMENTATION

The finger detecting process of the touch panel based on the MEFS sensing cells has three steps. Firstly, the common-mode capacitance and the differential capacitance of the sensing cell are measured. Secondly, based on the measured data, the touching status of the sensing cell is judged. Finally, based on the touching status, the accurate position of the finger is calculated. The details of the process are described as follows.

A. Capacitance measurement

The main part of the readout circuit to measure the capacitance of the MEFS sensing cell is shown in Fig. 6.

The readout circuit employs the switched-capacitor circuits [10], [11] rather than the oscillator based circuits [12]-[14] in consideration of power efficient. The analog front-end circuit structure of the readout circuit is shown in Fig. 6 (a), which is composed of two switched-capacitor readout circuits: differential capacitance to voltage convertor (DCVC) and common-mode capacitance to voltage convertor (CMCVC). The amplifiers used in DCVC and CMCVC are shown in Fig. 6(b) and Fig. 6(c), respectively. The clock phases are shown in Fig. 6(d). The analog front-end circuit has three distinctive features as described below.

Firstly, the differential capacitance and the common-mode capacitance are measured simultaneously and will not interfere with each other. In this structure, the DCVC, the CMCVC and the excitation are synchronized by the non-overlapping clock Clock-1 shown in Fig. 6 (d). When the excitation is active, the charge from the sensing cell is pumped into the readout circuit and is then divided into two parts. The differential part of the charge is absorbed by C_D and converted to the voltage V_D by DCVC. The common-mode part of the charge is absorbed by C_{CM} and converted to the voltage V_{CM} by CMCVC. That is,

$$V_D = \frac{C_1 - C_2}{C_D} V_R$$
$$V_{CM} = \frac{C_1 + C_2}{C_{CM}} V_R \quad (3)$$

The gains of DCVC and CMCVC are programmable to fit the sensing cell's capacitance, which are set by the programmable capacitor arrays C_D and C_{CM}.

Secondly, it employs the "Oversampling Successive Approximation" (OSA) technique [10], in order to suppress the output DC error brought by large grounded parasitic capacitance (i.e., C_{P1} and C_{P2} of the sensing cell shown in Fig. 1(c)). Also, this technique is able to reduce the DC offset brought by the process mismatch of amplifiers and the flicker noise in the low frequency range of amplifier. Both DCVC and CMCVC are implemented with the OSA technique. The circuit based on the OSA technique must be driven by the nested non-overlapping clock rather than traditional non-overlapping clock, as shown in Fig. 6(d), in order to minimize the charge injection from the switches. The principle of the OSA is explained later.

Thirdly, the inherent Sample-and-Hold (S&H) function of the circuit reduces power and chip area consumption. During the phase Φ2 of the clock, the capacitor C_H samples the outputs of DCVC and CMCVC. During the phase Φ1, the capacitor C_H forms a negative feedback loop with C_{OSA} to hold the outputs. Therefore, this function makes the readout circuit able to drive the ADC directly in phase Φ1 without a separate active S&H circuit, which saves power and chip area.

The OSA technique is described as follows [10]. As the MEFS sensing cell guides the high density electrical field into the ground, it introduces large parasitic capacitances to the ground, which appear as C_{P1} and C_{P2} in Fig. 1(c), Fig. 5 (a) and Fig. 6. The Fig. 5 shows the schematic of the traditional DCVC structure used as readout circuit [11]. The reference capacitors are used to absorb the common mode charge produced by C_1 and C_2. The output voltages of the traditional DCVC in the presence of the parasitic capacitance C_{P1} and C_{P2} are,

$$V_{D+}C_D = C_1\left(V_R - \frac{V_{D+} - V_{D-}}{A_1}\right) - C_{P1}\left(V_R + \frac{V_{D+} - V_{D-}}{A_1}\right)$$
$$V_{D-}C_D = C_2\left(V_R + \frac{V_{D+} - V_{D-}}{A_1}\right) - C_{P2}\left(V_R - \frac{V_{D+} - V_{D-}}{A_1}\right) \quad (4)$$

By transforming (4), the output is,

$$V_D = V_{D+} - V_{D-} = \frac{C_1 - C_2}{C_D} V_R \left(1 - \frac{1}{1 + A_1/\sigma}\right)$$
$$\sigma = \frac{C_1 + C_2 + C_{P1} + C_{P2}}{C_D} \quad (5)$$

where V_{D+} and V_{D-} are the two outputs of the traditional DCVC, A_1 is the gain of the operational amplifier, $1/(1 + A_1/\sigma)$ is the error term of the output voltage introduced by the parasitic capacitances. In general, C_{P1} and C_{P2} induced by sensing cells, PCB wires, ESD devices and bonding pads are within the range of 10pF~100pF, C_1 and C_2 are within the range of 20fF~200fF, C_D is 100fF and A_1 is within the range of 70dB~90dB. So the error would be 3.1%~24.0% according to (5), which would significantly reduce the accuracy of the readout circuit.

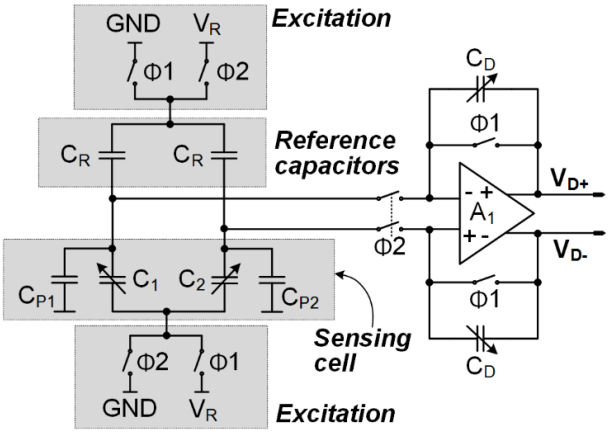

Fig. 5. The traditional DCVC used as the readout circuit for the MEFS sensing cell

However, in the OSA based DCVC, the above problem is solved. Instead of making the output reach its final value by one step, the OSA technique makes the output of DCVC reach its final value by several iteration steps. The capacitor C_{OSA} absorbs the error voltage in each iteration step, so that the output $V_D(n)$ will reach a high accuracy level with negligible error, as shown in Fig. 7. The detailed formulas are deduced below.

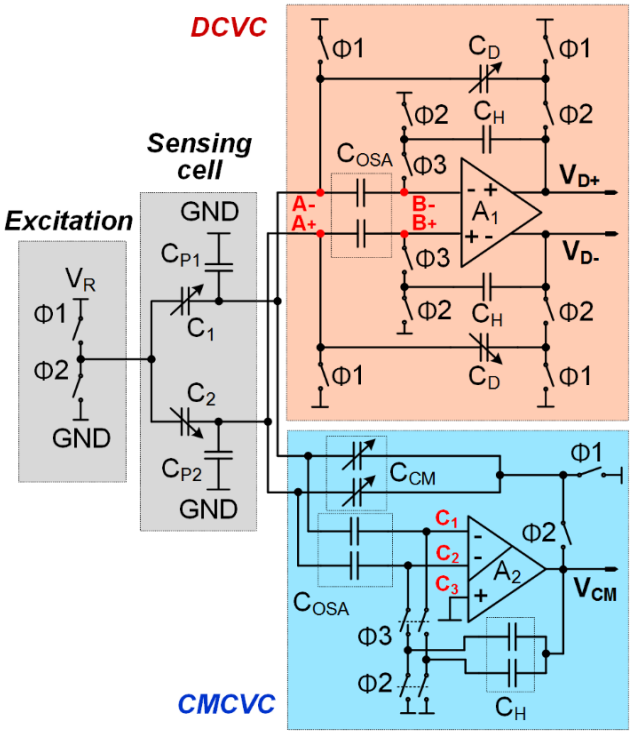

(a)

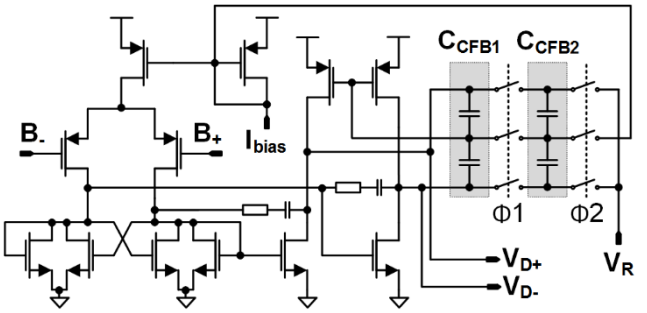

(b)

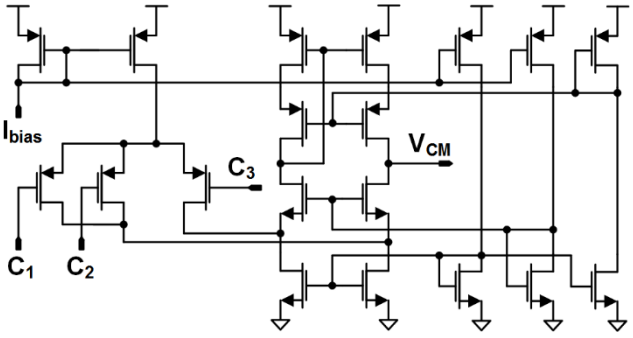

(c)

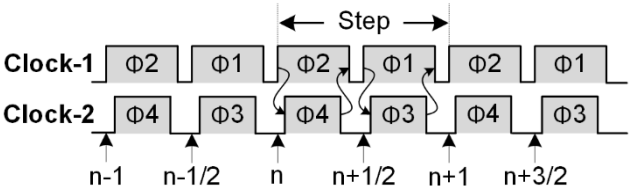

(d)

Fig. 6. The proposed circuit implementation of the readout circuit for the MEFS sensing cell. (a) The analog front-end of readout circuit. (b) The fully differential amplifier A1 used by readout circuit.(c) The common-mode amplifier A2 used by readout circuit .(d) The two-phase nested non-overlapping clocks diagram.

During the Φ2 of the 1st step, the increment of the output is $V_D(n)$. According to (5), the 1st level of the output voltage of DCVC in Fig. 7 (a) is

$$V_D(n) = \frac{C_1 - C_2}{C_D} V_R - \frac{\sigma}{A_1} V_D(n) \tag{6}$$

where the $\sigma V_D(n)/A_1$ is the error term caused by parasitic capacitances and the output increment $V_D(n)$. The reason why the error term appears is that the voltage difference between nodes A+ and A- (denoted by V_{A+A-}) is not zero, which leads to the error charge from the parasitic capacitances C_{P1} and C_{P2}.

Then during the next phase Φ1 of the 1st step in Fig. 7(a), the voltage difference V_{A+A-} is "absorbed" by the capacitor C_{OSA}. This is because the nodes A+ and A- are shorted to the ground while the V_{B+B-} remains at the same level due to the holding of the output level by the C_H. So the error in this step is eliminated, as shown in Fig. 7(b).

During the phase Φ2 in the 2nd step, the iteration takes place. As the "old" error in the 1st step produced by $V_D(n)$ is eliminated by the capacitor C_{OSA}, the "new" error in the 2nd step is produced by the increment value of the output in this step $\Delta V_D(n+1)$ rather than by the absolute value of the output this step $V_D(n+1)$, that is,

$$V_D(n+1) = \frac{C_1 - C_2}{C_D} V_R - \frac{\sigma}{A_1} \Delta V_D(n+1) \tag{7}$$

Similar to (7), the output levels of the other steps are,

$$V_D(n+2) = \frac{C_1 - C_2}{C_D} V_R - \frac{\sigma}{A_1} \Delta V_D(n+2)$$

$$\vdots$$

$$V_D(n+N) = \frac{C_1 - C_2}{C_D} V_R - \frac{\sigma}{A_1} \Delta V_D(n+N) \tag{8}$$

The relationship between the increment value and absolute value of two consecutive steps is

$$\Delta V_D(n+1) = V_D(n+1) - V_D(n) \tag{9}$$

By combining (6)-(9), the output in N-th step is,

$$V_D(n+N) = \frac{C_1 - C_2}{C_D} V_R \left[1 - \left(\frac{1}{1 + A_1/\sigma}\right)^{N+1}\right]$$

$$\sigma = \frac{C_1 + C_2 + C_{P1} + C_{P2}}{C_D} \tag{10}$$

Compared with (5), (10) shows that the error term $1/(1 + A_1/\sigma)$ is to be diminished and it tends towards zero exponentially with the increase of N. This means that the error will be reduced to infinitesimal regardless of the A_1 and the parasitic capacitances C_{P1} and C_{P2}, but this is at cost of settling time.

The capacitor C_{OSA} is the key component holding the error voltage, which should be charged accurately in order to guarantee the accuracy. Therefore, the nested non-overlapping clock (Clock-2) is used to control the charging process of the capacitor C_{OSA}. During the high level of the nested clock phase Φ3 when the capacitor C_{OSA} is being charged, all the other switches driven by the Clock-1 (phases Φ1 and Φ2) are inactive so as not to inject any interference charge into the capacitor C_{OSA}.

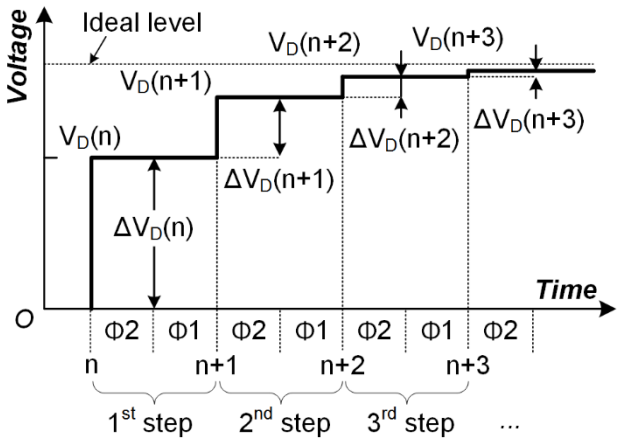

(a)

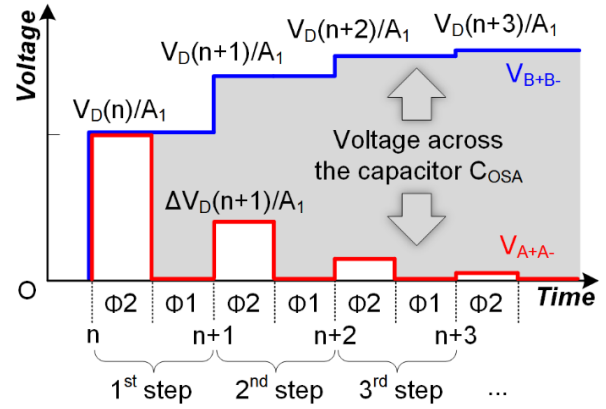

(b)

Fig. 7. The concept of OSA based DCVC approaching ideal level. (a) The process of output voltage approaching ideal level. (b) The process of diminishing of the error caused by the parasitic capacitance of MEFS sensing cell.

In terms of noise in capacitive touch panel, there are externally injected noise and internal circuit noise, and both of them severely deteriorate the signal-to-noise ratio (SNR) performance. The externally injected noise refers to the self-noise produced by the objects touching the panel and the display noise produced by the display screen under the touch panel. The power of externally injected noise depends on the power of the noise source and the value of coupling capacitor between the touch panel and the noise source [1]. In order to reduce the external injected noise, the coupling capacitance is reduced via inserting isolation layer with proper thickness between the touch panel and the noise source [2]. The internal circuit noise is dominated by the flicker noise in low frequency, since thermal noise in high-frequency range is limited by the system bandwidth. The flicker noise can be reduced by the OSA circuit in which the flicker noise is stored as an input equivalent noise in the capacitor C_{OSA} in phase Φ1 and is then cancelled in phase Φ2. This storing-and-cancelling process for the noise reduction of the OSA circuit is similar to that of the correlated double sampling (CDS) circuit. According to the reference [15], the normalized expression of the noise power spectral density in the CDS circuit is,

$$\left|H(e^{j\omega T})\right|^2 = \left|1 - z^{-1}\right|_{z=e^{j\omega T}} = 4\,sin^2\left(\frac{\omega T}{4}\right) \quad (11)$$

Equation (11) indicates that the magnitude is low when the frequency ω is low, which means that the noise power is suppressed in low frequency range (referring to the flicker noise).

The transistor-level numerical analysis results of the OSA based DCVC by SPICE are shown in Fig. 8. Here, the simulation conditions are $C_{OSA} = 3.5pF$, $C_H = 1.75pF$, $C_D = 180fF$, $C_{CFB1} = 100fF$, $C_{CFB2} = 300fF$ and $V_R = 900mV$, which means that the ideal output voltage level of the DCVC V_{ideal} is 200mV. When the value of the parasitic capacitances (C_{P1} and C_{P2} in Fig. 6 (a)) is 10pF, 100pF, 1000pF, respectively, the output voltage level of the OSA based DCVC driven by traditional non-overlapping clock V_{OSA_TC} is 202.3mV, 218.9mV, 416.4mV, respectively, the output voltage level of the OSA based DCVC driven by nested clocks V_{OSA_NC} is 199.99mV, 199.98mV, 199.8mV, respectively, and the output voltage level of the traditional DCVC [11] driven by traditional non-overlapping clock V_{TDCVC} is 202.1mV, 182.5mV, 102.6mV, respectively. The normalized output errors (i.e. the percentage difference between the V_{OSA_TC} and the V_{ideal}, the percentage difference between the V_{OSA_NC} and the V_{ideal}, and the percentage difference between the V_{TDCVC} and the V_{ideal}) varying with the parasitic capacitance are shown in Fig. 8 (d). It is clear that without nested clocks, the output error of the OSA based DCVC is similar to that of the traditional DCVC when parasitic capacitance is below 100pF (in most cases the parasitic capacitance will not exceed 100pF). In contrast, driven by the nested clocks, the output error of the OSA based DCVC is significantly reduced (for example, by 57dB from 10.02% to 0.015% when the parasitic capacitance is 100pF, compared to the traditional DCVC).

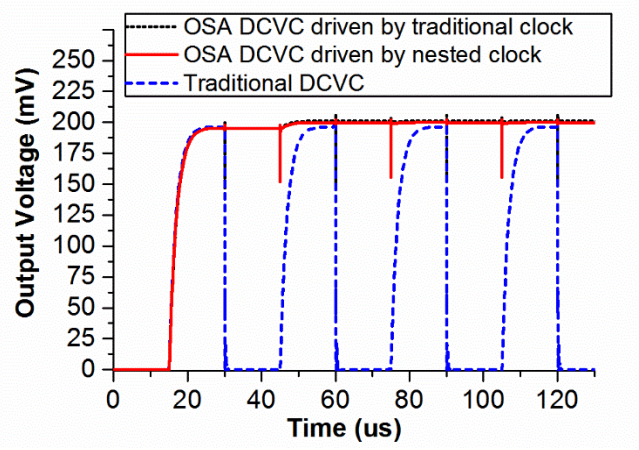

(a)

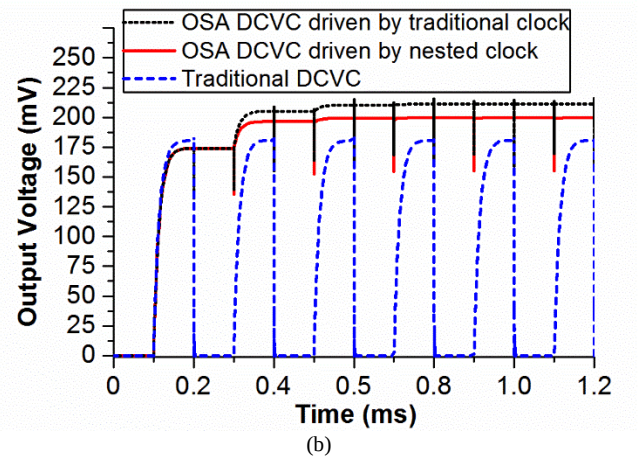

(b)

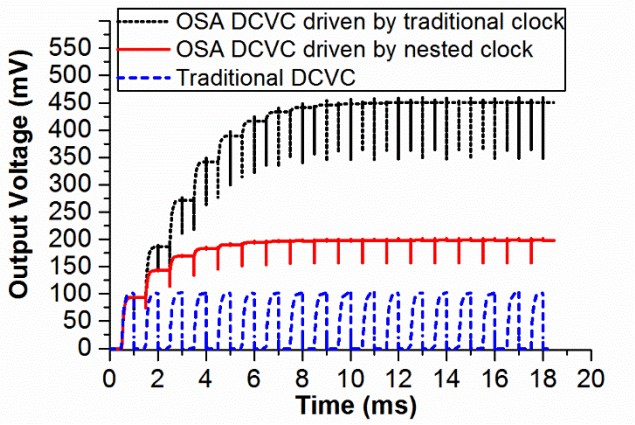

(c)

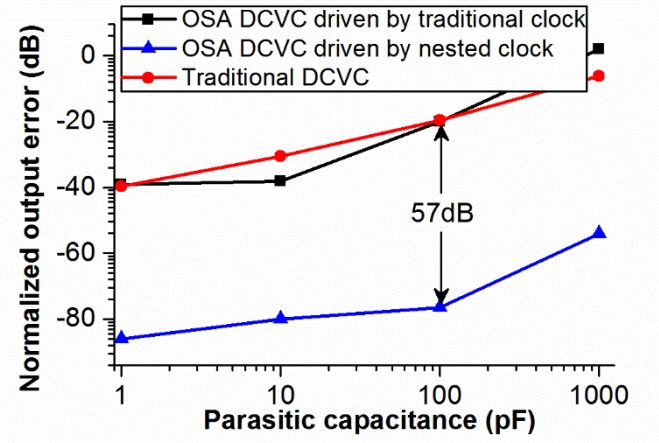

(d)

Fig. 8. The output of traditional DCVC, OSA based DCVC driven by traditional clock and OSA based DCVC driven by nested clock. (a) The output with 10pF parasitic capacitance. (b) The output with 100pF parasitic capacitance. (c) The output with 1000pF parasitic capacitance. (d) The normalized output error with parasitic capacitance varying from 1pF to 1000pF.

The accuracy of the OSA based CMCVC is similar to that of the OSA based DCVC. The process of diminishing the error caused by the parasitic capacitance is similar to that described by (6)-(10). The OSA based CMCVC should also be driven by the nested non-overlapping clocks rather than the traditional non-overlapping clock to achieve the high accuracy. With the simulation conditions of $C_{OSA} = 3.5pF$, $C_H = 1.75pF$ and $C_{CM} = 300fF$, the simulation result shows that the accuracy of the OSA based CMCVC driven by the nested clocks is improved by 55dB, compared with that of the OSA based CMCVC driven by the traditional clock.

B.Touching status judgment and finger position calculation

Based on the data outputted by the readout circuit, the touching status of the sensing cells is judged according to the characteristics of the cells illustrated in the section II.

The fully touched cells have the largest value of common-mode capacitance. If the common-mode capacitance of a sensing cell is beyond 200fF, this cell is thought to be fully touched by a human finger. An example of fully touched cell is Cell 5 shown in Fig. 9 (a). All of its four sensing plates (highlighted with color) are covered by the finger.

If the common-mode capacitance is below 30fF and the differential capacitance is beyond 30fF, this cell is thought to be partly touched in X-axis direction. The examples of partly touched cell in X-axis direction are Cell 5 shown in Fig. 9 (b) and Fig. 9 (c).

If the common-mode capacitance is between 30fF and 200fF and the differential capacitance is below 30fF, this cell is thought to be partly touched in Y-axis direction. The examples of partly touched cell in Y-axis direction are Cell 5 shown in Fig. 9 (d) and Fig. 9 (e).

All possible statuses of a sensing cell are listed in the table I. Notice that only in the fully touched status (status-B) can the MEFS sensing cell distinguish the finger from the water-drop, because the finger can make the common-mode capacitance rise beyond 200fF while the water-drop cannot. The partly touched statuses (status-C, D, E) may be caused by either water-drop or finger. So the status-B cells are used to distinguish finger from water-drop while the status-C, D, E cells are used to calculate the position of a finger. For example, if there is only water-drop, status-B will not be reported, as shown in Fig. 10 (a). As a result, the finger position calculation will not start.

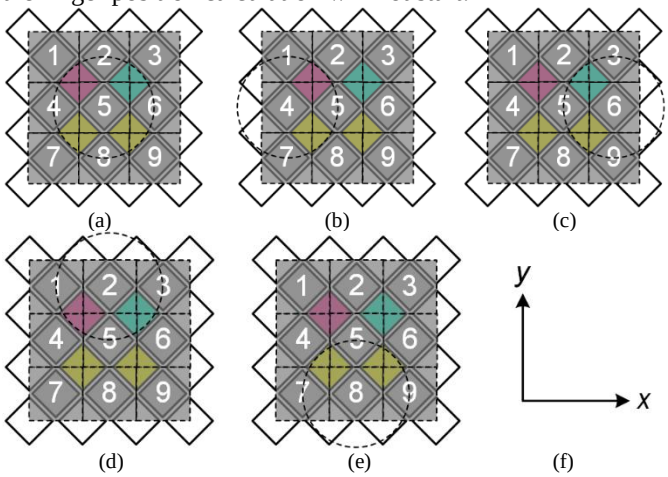

Fig. 9. The MEFS sensing cell in different touching statuses with its measurement plates highlighted. The circle represents the contacting area of the finger. (a) The Cell 5 is fully touched. (b) The Cell 5 is partly touched in negative x-axis direction. (c) The Cell 5 is partly touched in positive x-axis direction. (d) The Cell 5 is partly touched in positive y-axis direction. (e) The Cell 5 is partly touched in negative y-axis direction. (f) The coordinate setting.

TABLE 1 TOUCHING STATUS JUDGMENT

	Common-mode capacitance (fF)			Differential capacitance (fF)		Touching status
	<30	30-200	>200	<30	>30	
A	Y	-	-	Y	-	Not touched
B	-	-	Y	-	-	Fully touched by finger
C	-	Y	-	Y	-	Partly touched (Y) by finger or water
D	Y	-	-	-	Y	Partly touched (X) by finger or water
E	-	Y	-		Y	Partly touched (X&Y) by finger or water

When the status-B is reported, the finger position is calculated based on the statuses of the other sensing cells next to the status-B cell, as shown in Fig. 10 (b)-(d). The equations for calculation of the finger position are

$$x_{finger} = x_1 + \frac{a}{2}\frac{VD_{X-P} - VD_{X-N}}{VD_{X-P} + VD_{X-N}}$$
$$y_{finger} = y_1 + \frac{a}{2}\frac{VC_{Y-P} - VC_{Y-N}}{VC_{Y-P} + VC_{Y-N}} \quad (12)$$

where a is the side-length of the sensing cell; x_1 and y_1 are the x-axis position and y-axis position of the center point of the status-B cell, respectively; $VD_{X\text{-}N}$ and $VD_{X\text{-}P}$ are the displacements of status-D cells in the negative and positive X-axis directions of the status-B cell, respectively; $VC_{Y\text{-}N}$ and $VC_{Y\text{-}P}$ are the displacements of status-C cells in the negative and positive Y-axis directions of the status-B cell, respectively.

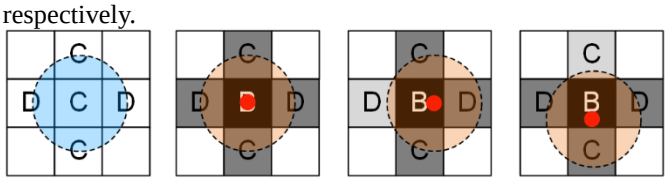

(a) (b) (c) (d)

Fig. 10. The calculation of the finger position based on the data from touching status judgment. (a) Finger position is not calculated as no status-B cell is detected; (b) Finger position is at the center of status-B cell; (c) Finger position is biased in the X-axis direction by status-D cells; (d) Finger position is biased in the Y-axis direction by status-C cells;

IV. EXPERIMENT RESULTS

The capacitive readout circuit is fabricated by the commercial 0.18μm Bipolar-CMOS process from Dongbu HiTek Co., LTD. This readout chip integrates the OSA based CMCVC, OSA based DCVC, Sigma-delta analog-to-digital convertor, reference voltage, reference current, clock generator and buffer circuit. The area and power consumption of the whole chip are 0.31mm^2 and 450μW (measurement data), respectively, where the area and power consumption of the CMCVC and DCVC which are essential components of the circuit to read sensing cell are 0.04mm^2 and 65μW (simulation data), respectively. The power consumptions of each of the above building blocks is shown in Fig. 11.The summary data of the readout IC is shown in the Table II. In order to read different types of sensing cells (i.e., the traditional sensing cell and the MEFS sensing cell), two sensitivity measurements are taken to reflect the different circuit parameters used for the different sensing cells. The noise floor is measured when the IC is not connected to sensing cell. Similar to the Common-Mode Rejection Ratio (CMRR) which is used to quantify the ability of amplifier to reject common-mode interference, the Parasitic Capacitance Rejection Ratio (PCRR) is defined to quantify the ability of the readout circuit to reject common-mode parasitic capacitance [10], [16], [17] i.e.,

$$PCRR = 20\log\left(\frac{S_{par}}{S_{\Delta C}}\right) \tag{13}$$

where $S_{\Delta C}$ is the sensitivity to the capacitance of the sensing cell and S_{par} is the sensitivity to the parasitic capacitance. In this work, $S_{\Delta C}$ is 5mV/fF and S_{par} is 3mV/nF. According to (13), the PCRR of the OSA readout circuit is -124.4dB. The measurement of S_{par} is shown in Fig. 12. The discrete capacitors (1nF-10nF) are used to simulate parasitic capacitance in the measurement. When two discrete capacitors, each with a value of 10nF, are connected, the output of ADC is 1.07V. Then the 10nF capacitors are cut off and the output of ADC changes by 30mV from 1.07V to 1.10V. The chip is tested with different discrete capacitor values (1.0nF, 2.2nF, 4.7nF and 10nF) in order to obtain a reliable S_{par}.

The PCRR of this work is much better than that of the references [16] and [17], which are -68.6dB and -44.2dB, respectively. This verifies the theoretical analysis in the section III that the OSA technique performs well in reducing the interference of the common-mode parasitic capacitance. The PCRR of this work is also better than that of the reference [10] (PCRR= -80dB) where the OSA technique is firstly proposed. This is because the reference [10] uses single stage amplifier (38dB) whose gain is much lower than that of the amplifier used in this work (87dB), and the low amplifier gain leads to low PCRR, according to the non-idealities explained in the reference [10]. Furthermore, while the reference [10] focused on the ability of OSA technique to relax the gain requirement of the amplifier, this work focuses on the ability of OSA technique to reduce the sensitivity to common-mode parasitic capacitance.

TABLE II BASIC PARAMETERS OF THE READOUT IC

Parameters	Values
Chip area	0.31mm^2
Supply voltage	1.8V
Power consumption	450uW
Sensitivity of DCVC	1mV/fF, 5mV/fF
Sensitivity of CMCVC	1mV/fF, 5mV/fF
Noise (peak-to-peak value)	12mV
PCRR	-124.4dB

The touch panel based on the traditional sensing cells and the touch panel based on the MEFS sensing cells are fabricated on a PCB with 9 sensing cells, which covers an area of 2cm×2cm, as shown in Fig. 13. The wire routing of the touch panel based on MEFS sensing cells is more complex than that of the traditional one, due to the addition of ground plates. As a result, the touch panel based on MEFS sensing cells need one more layer for wire routing than the traditional one does.

The experiment to verify the ability of this system to distinguish water drop from human finger is shown in Fig. 13 and the moving traces are shown in Fig. 14. The readout circuit is connected to the central sensing cell of the touch panel, and other sensing cells are connected to the ground. For the traditional structure, when the finger or the water-drop (7mm in diameter) moves from the position 0 to 6 in x-axis direction with the y-axis position being 3, the outputs of DCVC and CMCVC are shown in Fig. 15 (a) and Fig. 15 (b), respectively. When the finger or the water-drop moves from position 0 to position 6 in y-axis direction with the x-axis position being 3, the outputs of DCVC and CMCVC are shown in Fig. 15 (c) and Fig. 15 (d), respectively. The same test procedure is conducted on the MEFS structure, and the results are shown in Fig.13 (e) - (f).

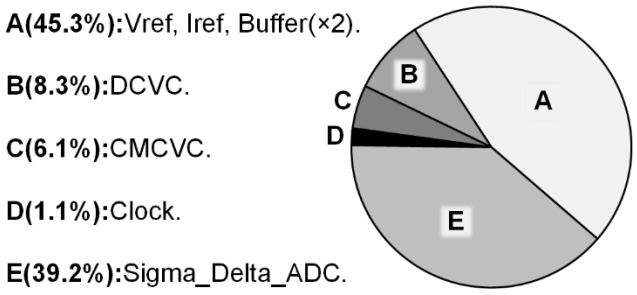

Fig. 11. The power consumption of each building blocks.

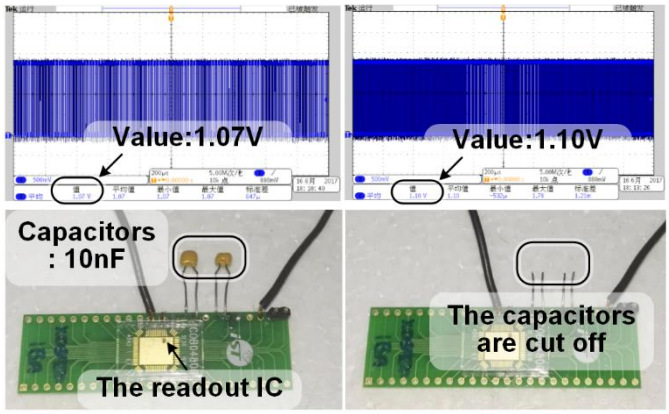

Fig. 12. The measurement of the sensitivity to common-mode parasitic capacitance or PCRR.

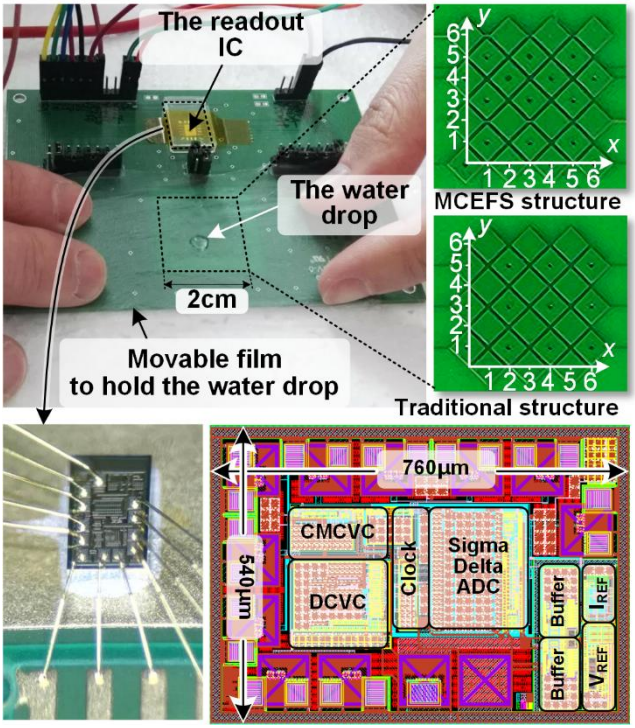

Fig. 13. The test environment, fabricated touch panels and readout IC

The results in Fig. 15 (a)-(d) show that when traditional sensing cell is fully touched by water-drop and finger, respectively, the outputs of the CMCVC are 1.32V and 1.33V, as indicated by the point (x=3, y=3) in Fig. 15(b). So the percentage difference between the output voltages of these two cases is only 0.75%, which means that the traditional sensing cell can hardly distinguish the finger from the water-drop.

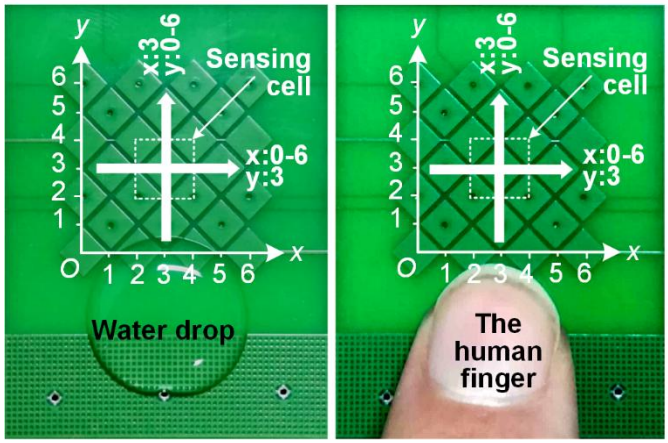

Fig. 14. The test configuration. The white arrows are the moving traces of the touching objects.

However, when the MCESF sensing cell is fully touched by water-drop and finger, respectively, the outputs of the CMCVC are 1.11V and 1.23V, as indicated by the point (x=3, y=3) in Fig. 15(f). So the percentage difference between the output voltages of these two cases is 9.7%, which is a very significant improvement compared to that of the traditional sensing cell (0.75%). When the finger moves along the x-axis, the measured data from the DCVC between the position 2 and 4 in Fig. 15 (e) can be used for calculating the x position of the finger using (12). When the finger moves along the y-axis, the measured data from the CMCVC between position 2 and 4 in Fig. 15 (h) can be used for calculating y position using (12).

It is therefore evident that compared with the traditional sensing cell, the proposed MEFS sensing cell has a much lower sensitivity to the interference of water-drop in the detection of the finger.

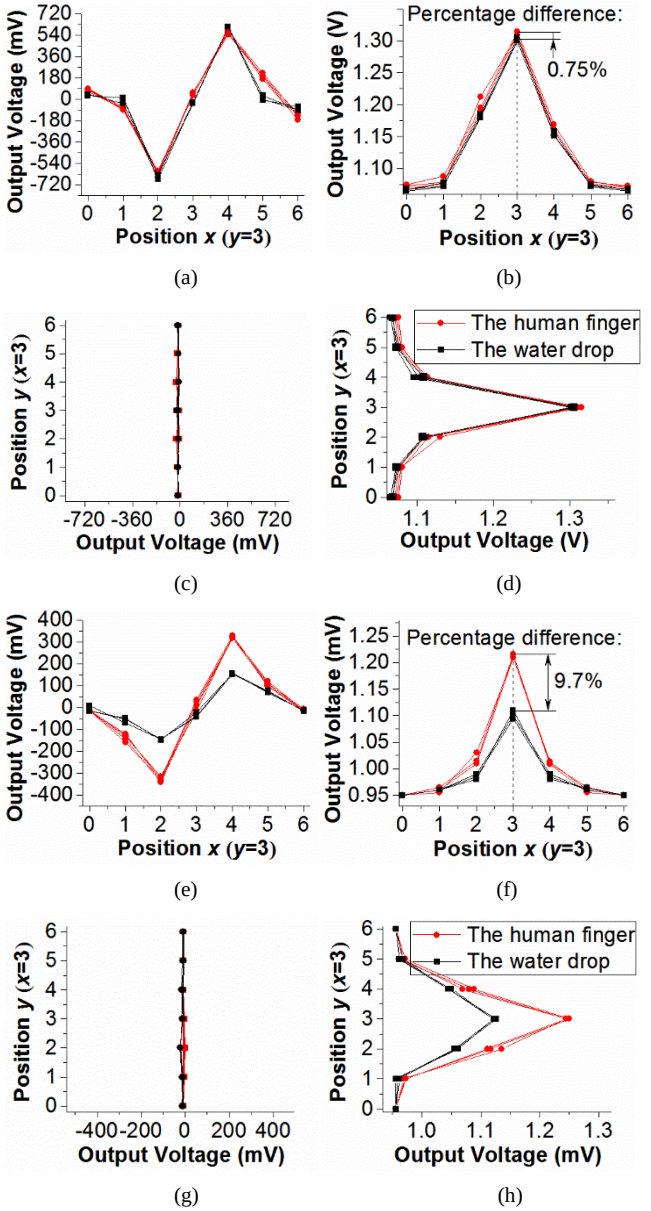

Fig. 15. The measurement results of the traditional and MEFS touch panel touched by the finger and the water-drop. (a) Traditional DCVC output in x-axis (left). (b) Traditional CMCVC output in x-axis. (c) Traditional DCVC output in y-axis. (d) Traditional CMCVC output in y-axis. (e) OSA based DCVC output in x-axis. (f) OSA based CMCVC output in x-axis. (g)

OSA based DCVC output in y-axis. (h) OSA based CMCVC output in y-axis.

The comparison of this work with the similar works [1], [2], is shown in Table III. The main contribution of this work is the implementation of its ability to distinguish the water drop from the human finger. However, this is at the cost of power consumption and SNR. The power consumption of this work is higher and it is due to the CMCVC which was not used in the other works. The SNR of this work is lower than that of the other works. This is because the maximum signal level is small. The small maximum signal level is the result of the reduction of the sensitivity of the MEFS sensing cell, which is caused by the addition of ground plates.

TABLE III COMPARISON OF THIS WORK TO THE OTHERS

Items	[1]	[2]	This work
Sensing cell type	Differential mutual-capacitance	Self-capacitance	**Proposed MEFS sensing**
Water distinguish ability	**No**	**No**	**Yes**
IC process	3.3V 0.35um BCD	1.2V/5.5V/30V 110nm BCD	1.8V 0.18um BCD
Power*	28uW	35uW	65uW
SNR	43.5dB	51dB	36dB**
Scan ratio	120Hz	120Hz	120Hz***

* Power consumption is acquired by calculating the circuit blocks (CMCVC and DCVC) which are specialized for a single sensing cell.
** The peak-to-peak noise is 12mV which is equal to a RMS noise of 2mVrms [15]. The maximum signal level is 120mV. As a result, the SNR is 36dB.
*** The scan ratio is determined by the settling time. The settling time of OSA circuit is shorter than 8.3ms, so it can support 120Hz scan ratio.

V. CONCLUSIONS

The MEFS sensing cell is proposed in this paper which significantly improves the touch panel's ability to distinguish water-drop from human finger. The readout IC for the MEFS sensing cell is also designed and fabricated using 0.18um CMOS process. The touch panel with 9 sensing cells and the readout IC are integrated into a PCB board-level system. The test results of the system show that for the MEFS sensing cell, the percentage difference between the output voltages is 9.7%, i.e., 0.12V (1.23V-1.11V) when the sensing cell is touched by the water-drop and the finger, respectively, while it is only 0.75%, i.e., 0.01V (1.33V-1.32V), for the traditional sensing cell. This demonstrates that compared to the traditional sensing cell, the MEFS sensing cell has achieved a very significant improvement on the ability to reduce water-drop interference.

REFERENCE

[1] S. Park, H. Kim, J. Bang, G. Cho and G. Cho, "A 0.26-nJ/node, 400-kHz Tx Driving, Filtered Fully Differential Readout IC With Parasitic RC Time Delay Reduction Technique for 65-in 169×97 Capacitive-Type Touch Screen Panel", *IEEE J. Solid-State Circuits*, vol. 52, no. 2, pp. 528-542, Feb. 2017.

[2] J. Jun, B. Kim, S. Shin, K. Jang, J. Baek and C. Kim, "In-Cell Self-Capacitive-Type Mobile Touch System and Embedded Readout Circuit in Display Driver IC," *Journal of Display Technology*, vol. 12, no. 12, pp. 1613-1622, Dec. 2016.

[3] Kremin V, Kulyk T, Karpin O, et al. Reducing water influence on a touch-sensing device: US patent, US8717331[P]. 2014.

[4] Faller L M, Mühlbacher-Karrer S, Zangl H. "Inkjet-printing rapid prototyping of a robust and flexible capacitive touch panel". *2016 IEEE SENSORS*, Orlando, FL, 2016, pp. 1-3.

[5] Won D J, Baek S, Huh M, et al. "Robust capacitive touch sensor using liquid metal droplets with large dynamic range". *Sensors & Actuators A Physical*, pp:105-111. 2017.

[6] Jiang X Z, Sun Y J, Fan Z, et al. Integrated Flexible, "Waterproof, Transparent, and Self-Powered Tactile Sensing Panel". *Acs Nano*, vol.10, no.8, pp. 7696–7704. 2016.

[7] Chen Z, Luo R C. "Design and implementation of capacitive proximity sensor using micro-electromechanical systems technology". *IEEE Transactions on Industrial Electronics*, vol.45, no.6, pp. 886-894. 1998.

[8] Thoresen C B, Hanke U. "Numerical Simulation of Mutual Capacitance Touch Screens for Ungrounded Objects". *IEEE Sensors Journal*, PP (99):1-1. 2017.

[9] M Miyamoto, M Hamaguchi. "A Nagao. A 143× 81 Mutual-Capacitance Touch-Sensing Analog Front-End With Parallel Drive and Differential Sensing Architecture". *IEEE J. Solid-State Circuits*, vol.50, no.1, pp. 335-343. 2014.

[10] L. Zhong, X. Lai and D. Xu, "Oversampling Successive Approximation Technique for MEMS Differential Capacitive Sensor," *IEEE J. Solid-State Circuits*, vol. 53, no. 8, pp. 2240–2251, May. 2018..

[11] Xu H, Liu X, Yin L. "A Closed-Loop Σ Δ Interface for a High-Q Micromechanical Capacitive Accelerometer with 200 ng/√Hz Input Noise Density". *IEEE J. Solid-State Circuits*, vol.50, no.9, pp. 2101-2112, 2015.

[12] Zhao J. "A 0.23 μg Bias Instability and 1.6 μg/sqrt(Hz) Resolution Silicon Oscillating Accelerometer with Build-in Σ-Δ Frequency-to-Digital Converter", *2016 IEEE Symposium on VLSI Circuits (VLSI-Circuits)*, Honolulu, HI, 2016, pp. 1-2.

[13] J. Zhao et al., "A System Decomposition Model for Phase Noise in Silicon Oscillating Accelerometers," *IEEE Sensors Journal*, vol. 16, no. 13, pp. 5259-5269, July1, 2016.

[14] J. Zhao et al., "A 0.23- g Bias Instability and 1-ug /√Hz Acceleration Noise Density Silicon Oscillating Accelerometer With Embedded Frequency-to-Digital Converter in PLL," *IEEE J. Solid-State Circuits*, vol. 52, no. 4, pp. 1053-1065, April 2017.

[15] Tony Chan Carusone, David Johns, Kenneth Martin. "Analog Integrated Circuit Design", 2nd ed.. USA: John Wiley & Sons, Inc., 2012, pp. 557-605.

[16] Nizza N, Dei M, Butti F, et al. "A Low-Power Interface for Capacitive Sensors with PWM Output and Intrinsic Low Pass Characteristic". *IEEE Trans. Circuits Syst. I, Reg. Papers*, vol.60, no.6, pp. 1419-1431. 2013.

[17] Scotti G, Pennisi S, Monsurrò P, et al. "88μA 1-MHz Stray-Insensitive CMOS Current-Mode Interface IC for Differential Capacitive Sensors". *IEEE Trans. Circuits Syst. I, Reg. Papers*, vol.61, no.7, pp. 1905-1916. 2014.

Longjie Zhong (M'18) received the BSc. degree in Biomedical Engineering in Xidian University, Xi'an, China, in 2012. He is currently pursuing the Ph.D. degree in Electronic Engineering at the Xidian University. Since 2017, he is also a Visiting Student of Nanyang technological university, Singapore. His research interests are high performance analog design in scaling CMOS and the sensor interface for IoE application.

Xinquan Lai (M'18) received the BSc and MSc degrees from School of Electronic Engineering, Xidian University, Xi'an, China, in 1987, 1993 respectively, and he received Ph.D. degree from School of Computer, Northwestern Polytechnical University, Xi'an, China, in 1998. He is currently a professor in the School of Electronic Engineering at Xidian University. His main research interests include mixed-signal integrated circuit for MEMS inertial sensors, light sensors, microphone, Class-D audio amplifier, LED/LCD driver, motor driver, battery charge controller and SoC systems for Wireless communication.

Donglai Xu (M'99-SM'06) received the BSc and MSc degrees in Electronic Engineering from Xidian University, China in 1985 and 1990, respectively, and the PhD degree in Electronic and Electrical Engineering from the University of Bradford, UK in 1999. Since 1998, Dr Xu has been with Teesside University, UK, where he is a Reader in Electronic Engineering. His research interests include video signal processing, circuits and systems design, VLSI and organic electronic devices. Since 2013, Dr Xu is also a Visiting Professor of Wuhan Polytechnic University, China.

Xinqin Liao received his BS degree from Fuzhou University in 2012 and his PhD from University of Science and Technology Beijing in 2017. Currently, he is a Research Fellow at Nanyang Technological University, Singapore. His research interests mainly focus on fabricating wearable devices for human-machine interactions.

Chuanshi Yang, received the B.Sc. degree in Shandong University, P. R. China in 2012. M. Eng. from Southeast University, P. R. China in 2015. He is currently pursuing the Ph.D. degree in Nanyang Technological University in Singapore. His current research interests include the high resolution low power ADC and interface circuits for ultrasound sensors.

Zhongyuan Fang attained B.Sc. with microelectronics at Fudan University in 2016. He is currently pursuing the Ph.D. degree with full scholarship in Electrical and Electronic Engineering Department, Nanyang Technological University, Singapore. Since Jul. 2016, he has been in Virtus IC Design Center of Excellence, Singapore. From 2014 to 2016, he was an undergraduate Research Assistant at State Key Laboratory of ASIC and System, Shanghai. His research interests include analog/mixed signal and low-power integrated circuit design, energy-efficient algorithms for physiological signal extraction, AI enabled IC design, as well as RF/Wireless communication circuits and systems design and testing for biomedical applications. Mr. Fang was awarded the Excellent Student Scholarship from Fudan University in 2016. He is also the recipient of the Fudan Science and Technology Innovation Award based on his work on the NSFC supported 802.11ah transceiver design. He got the highest grade on his B.S. graduation thesis. His work has been published in ISSCC, ISCAS.

Yuanjin Zheng (M'02) received the B.Eng. and M.Eng. degrees from Xi'an Jiaotong University, Xi'an, China, in 1993 and 1996, respectively, and the Ph.D. degree from the Nanyang Technological University, Singapore, in 2001. From July 1996 to April 1998, he was with the National Key Laboratory of Optical Communication Technology, University of Electronic Science and Technology of China. In 2001, he joined the Institute of Microelectronics (IME), Agency for Science, Technology and Research (A*STAR), Singapore, as a Senior Research Engineer, and was then promoted to a Principle Investigator. With the IME, he has led and developed various projects like CMOS RF transceivers, baseband system-on-a-chip (SoC) for wireless local area networks (WLANs), WCDMA, ultra-wideband (UWB), and low-power medical radio, etc. In July 2009, he joined the Nanyang Technological University and at present he is an Associate Professor. His research interests are gigahertz RFIC and SoC design, UWB systems and circuits, bio-IC systems and circuits, adaptive signal and image procession algorithms, and application-specific integrate circuits (ASICs). 300 journal and conference papers, 26 patents filed/granted and 5 book chapters. He is IEEE senior member.